Publisher's note: This paper originally appeared in Journal of Biomedical Optics ***6****(3), 273–276 (July 2001). Figures 2 and 3 were printed in black and white in that issue but were intended to be in color. Thus, the paper is being reprinted in its entirety here with the figures in color.*

Z-polarized confocal microscopy

Nils Huse
Andreas Schönle
Stefan W. Hell
Max-Planck-Institute for Biophysical Chemistry
High Resolution Optical Microscopy Group
D-37077 Göttingen, Germany

Abstract. In light microscopy the transverse nature of the electromagnetic field precludes a strongly focused longitudinal field component, thus confining polarization spectroscopy and imaging to two dimensions (*x,y*). Here we describe a simple confocal microscopy arrangement that optimizes for signal from molecules with transition dipoles oriented parallel to the optic axis. In the proposed arrangement, we not only generate a predominant longitudinally (*z*) polarized focal field, but also engineer the detection scheme in such a way that in a bulk of randomly oriented molecules, the microscope's effective point-spread function is dominated by the contribution of those molecules that are oriented along the optic axis. Our arrangement not only implicitly allows for the determination of the orientation of transition dipoles of single molecules in three dimensions, but also highlights the contribution of *z*-oriented molecules in three-dimensional imaging.
[DOI: 10.1117/1.1382610]

Keywords: single molecule spectroscopy; longitudinal field; microscopy; confocal; transition dipole; *z* polarization.

Paper FM-06 received Mar. 31, 2001; revised manuscript received Apr. 2, 2001; accepted for publication Apr. 17, 2001.

1 Introduction

Absorption and fluorescence light microscopy are largely equivalent to the spatial mapping of molecular dipole transitions at high resolution. Most molecules feature a linear transition dipole moment $\boldsymbol{\mu}$ in which case the transition rate is proportional to $|\boldsymbol{\mu}\cdot\mathbf{E}|^2$, whereby $\mathbf{E}\equiv(E_x,E_y,E_z)$ defines the electric field in the focus.[1] Since the rate depends on the mutual orientation of the two vectors, controlling the orientation of the field **E** is highly desirable. This is readily accomplished in a spectrometer with two orthogonal, low aperture lenses; this principle has also been successfully applied in confocal imaging.[2,3] However, when flat sample mounting conditions and high collection efficiency are required an orthogonal lens arrangement is impossible. In this case, the transverse nature of light precludes a strong component E_z along the optic axis. As the μ_z component is less accessible, molecules whose transition dipoles are chiefly oriented in the *z* direction will absorb less. Moreover, the lack of a *z*-polarized diffraction maximum prevents the measurement of the full orientation of $\boldsymbol{\mu}$ at high spatial resolution, which is of particular concern in single molecule spectroscopy.[4–6] Significant longitudinal fields are created in surface-bound near-field optical microscopy,[7] but the results obtained by this method are entangled with proximity effects. In high-resolution far-field microscopy, the convenient determination of $\boldsymbol{\mu}$ is regarded as difficult.[8]

Electromagnetic focusing theory[9] reveals that the spherical curvature of the wave front gives rise to a longitudinal component E_z, which received some attention in high aperture confocal[10,11] and 4Pi-microscopy theory.[12] However, in these works E_z never was of primary importance because the orientation in the focal maximum is that of the incoming wave. Catalyzed by the observation of strong longitudinal fields in near-field optics and the desire to establish the three-dimensional (3D) orientation of the transition dipole of a molecule, longitudinal orientations in focused light fields recently became of strong interest to single-molecule spectroscopy and near-field optics.[13,14] In an interesting study, free-space modes with radially polarized fields[15,16] were calculated, and it was shown that these fields are accompanied by significant *z*-polarized components. In this arrangement, however, the *z*-polarized field was still of the order of its *x* and *y* counterparts. Comparatively strong *x* and *y* components are not disturbing when ''imaging'' spatially *isolated* point objects such as individual single molecules, because the difference between their spatial structure facilitates the spatial separation of their individual contribution. In other words, the *x*, *y* and *z* components produce characteristic spatial patterns of fluorescence that can be readily distinguished.

In recent calculations it was shown that parabolic mirrors also lead to major longitudinal fields because of their strong amplitudes at high focusing angles; the application of a confocal pinhole was considered in these studies,[17] as was also the potential application of this scheme for 3D imaging. However, the definition of an imaging mode producing a measured signal that is predominantly due to the *z*-polarized field has

Address all correspondence to Dr. Stefan W. Hell. E-mail: shell@gwdg.de

1083-3668/2001/$15.00 © 2001 SPIE

not been tackled. The z-polarized microscope (ZPM) proposed herein is technically robust and employs only one or two binary phase plates and a polarizer. Engineering the effective point-spread function (PSF)[18] with a suitable detection PSF creates a microscope with a signal *primarily* stemming from molecules with strong μ_z.

2 Concept and Results

Our theoretical studies of ZPM are performed by calculating the focal field with the Huygens–Fresnel principle[19]

$$\mathbf{E}(x,y,z)=A\int_0^{\alpha}\int_0^{2\pi}P(\phi)\sqrt{\cos\theta}\,\mathbf{E}'(\theta,\phi)e^{iks(\theta,\phi)}\times\sin\theta\,d\theta\,d\phi, \tag{1}$$

where α denotes the semiaperture angle, A a constant, and the angles (θ,ϕ) point on the Gaussian reference sphere. If the field is linearly polarized in the x direction, the field $\mathbf{E}'(\theta,\phi)$ across the wave front is

$$\mathbf{E}'(\theta,\phi)=\begin{pmatrix}\sin^2\phi+\cos^2\varphi\cos\theta\\ \sin\phi\cos\phi(\cos\theta-1)\\ \cos\phi\sin\theta\end{pmatrix}. \tag{2}$$

The formula

$$s(\theta,\phi)=\sqrt{f^2+\rho^2+z^2-2f(\rho\sin\theta\cos(\phi-\phi_P)+z\cos\theta)}$$

is the distance between a point on the wave front and a point in the image space (x,y,z); $\rho=\sqrt{x^2+y^2}$ and $\phi_P=\arctan(y/x)$. The term f denotes the focal length of the system. $P(\phi)$ is a phase function across the entrance pupil, which we seek to modify to enhance E_z.

In regular focusing, E_z vanishes along the optic axis because the z components that are symmetric with respect to the optic axis are reverted in sign. Figure 1 shows an arrangement generating a focal electric field with a predominant E_z component. An x-polarized, plane wave front passes a phase plate inducing a phase shift of π between the upper $(x>0)$ and lower $(x<0)$ half of the beam, so that $P(\phi)=\mathrm{sign}(\cos\varphi)$. The beam then passes an annulus covering a centered circular area of 90% of the total aperture, thus ensuring that the illumination occurs exclusively with rays that are strongly bent with respect to the axis. Due to the phase step, the z-oriented components are now in phase at the optic axis, whereas those of the x- and y-oriented components vanish for the same reason. Evidently, a semiaperture angle $\alpha\to 90°$ would produce the strongest z-polarized field; however, in this study we confine ourselves to $\alpha=67.3°$ which corresponds to an oil immersion lens of 1.4 numerical aperture. We elect a wavelength $\lambda=500$ nm; results for other wavelengths can be gained by simple scaling.

Figure 2 shows the intensity PSF $|\mathbf{E}|^2\equiv|(E_x,E_y,E_z)|^2$ when introducing the above phase plate. By comparing $|E_x(x,y,z=0)|^2$ and $|E_y(x,y,z=0)|^2$ with $|E_z(x,y,z=0)|^2$, shown in (a), (b), and (c), respectively, we contrast the intensity distribution of the transverse components with that of the longitudinal component in a quadrant of the focal plane. They fundamentally differ from the distribution of a regular high-aperture lens: E_x and E_y vanish at the focal point and their

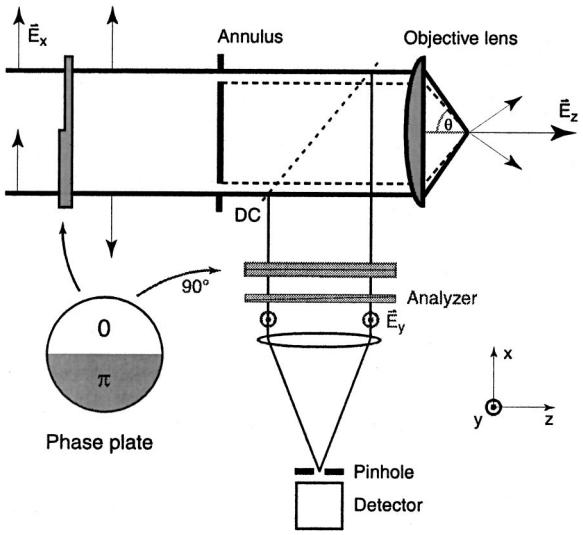

Fig. 1 Z-polarized light microscope (ZPM). A linearly x-polarized wave front passes a phase plate inducing a phase shift of π along the direction of polarization. Rays sustaining a large focusing angle θ are used by employing an annular aperture. The net effect is a longitudinally (z) polarized main diffraction maximum that can excite molecules with a predominantly z-polarized transition dipole. An analyzer and phase plate rotated by 90° in a confocal detection path lead to a detected fluorescence signal that stems predominantly from z-oriented molecules in the focal center.

main peak is shifted off axis. The calculations show that $|E_y|^2\leq 8.24\%$ and $|E_x|^2\leq 76.5\%$. Molecules with a substantial $\mu_{x,y}$ are excited when slightly offset from the focal point, which is not desired. However, the main maximum is indeed z polarized [Figure 2(c)] with a full width half maximum (FWHM) of 110 nm in the x and a FWHM of 160 nm in the y direction. It is accompanied by higher order side maxima with relative intensities of 51.8% and 20.8% in the x direction. Clearly, the insertion of a simple phase plate produces a pronounced main maximum that is entirely polarized in the z direction.

An immediate benefit is that the relative strengths of the components $\mu_{x,y,z}$ of a molecule can now be quantified by creating distinct field orientations in the diffraction maximum. For this purpose one subsequently records a set of three "xy images" of a molecule with focal spots of x, y, and z polarization, respectively; the x- and y-polarized PSFs are readily created by removing the phase plate and rotating the field with a retarder. Since the molecule is much smaller than the focal dimensions, the center of symmetry of the xy images coincides with the focal center, in which the molecule experiences a field that is exclusively x, y, or z polarized. One has to take into account that, due to the different distribution, in the z-polarized PSF the intensity at the focal point is 0.701 times smaller than for x and y polarization, so that the fluorescence generated by this PSF should be multiplied by 1.42. The full orientation of a linear molecular transition dipole can be determined with high spatial definition.

So far, our study applies to conventional and scanning microscopy. Although the maximal intensity of the z component is stronger by a factor 1.31 than that of its x-polarized counterpart, Figure 2 reveals that the latter is still strongly pro-

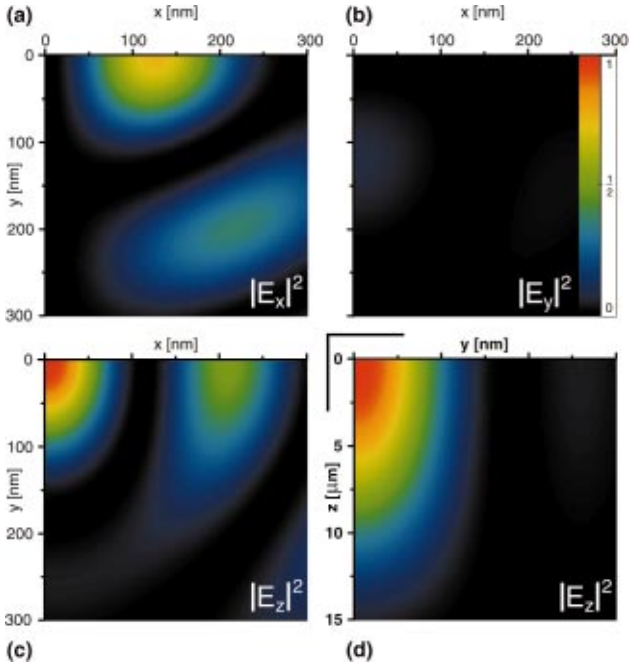

Fig. 2 Excitation intensity point-spread function in annular ZPM. Panels (a)–(c) show the intensity distribution of the *x*-, *y*- and *z*-oriented field components in the focal plane, respectively. Panel (d) shows an *xz* cross section of the *z* component. Panels (c) and (d) demonstrate that the main maximum is *z* polarized. The color look-up table applies to all figures.

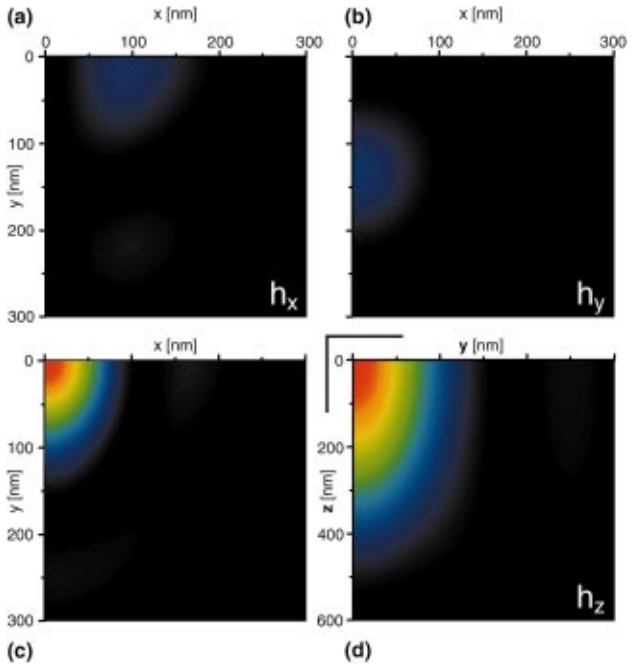

Fig. 3 Effective PSF of an annular illumination confocal ZPM enables *z*-polarized fluorescence microscopy with high spatial resolution. Panels (a)–(c) reveal the contribution to the signal from the *x*-, *y*-, and *z*-oriented field in the focal plane, respectively. The *xz* section of the longitudinal contribution exhibits the high spatial resolution of ZPM in (d).

nounced. In addition, the *z*-polarized field features significant lobes. To create a microscope with a predominant longitudinal field contribution, we now confocalize the microscope in a special manner. We implement a detection path that is similar to that for excitation (Figure 1) but rotate the phase plate by 90° and insert an analyzer pointing in the *y* direction. Another distinct difference to the illumination path is that we do not employ an annulus. By denoting the emitted field with **F** we obtain for the contribution probability of an arbitrarily oriented molecule with fixed transition dipoles

$$h(x,y,z) = C_1 \cdot \int_0^{\pi} \int_0^{2\pi} |\mathbf{E}\cdot\boldsymbol{\mu}|^2 |\mathbf{F}\cdot\boldsymbol{\mu}|^2 \sin\theta_d \, d\theta_d \, d\varphi_d$$

$$= C_2 \cdot \left(h_x + h_y + h_z + \sum_{i<j} h_{ij} \right) \tag{3}$$

with

$$h_i = |E_i|^2 \cdot (|F_i|^2 + \tfrac{1}{3}|F_j|^2 + \tfrac{1}{3}|F_k|^2),$$

$$h_{ij} = \tfrac{4}{3}\Re\{E_i E_j^*\}\Re\{F_i F_j^*\} \quad \text{for } (i \neq j \neq k) \in \{x,y,z\}$$

and $\boldsymbol{\mu} \equiv (\cos\varphi_d \sin\theta_d, \sin\varphi_d \sin\theta_d, \cos\theta_d)$. $\Re\{\}$ denotes the real part. Importantly, the rotated phase plate causes strong contributions from E_x to match low values F_y but E_z and F_z to coincide favorably in space (see Figure 2), so that contributions of the longitudinal field to the signal, h_z, will be emphasized. The "mixed contributions" h_{ij} are calculated to be negligible. The integral is performed over all dipole orientations in space, so that Eq. (3) gives the probability of an indefinitely oriented molecule to contribute to the signal. Therefore, the expression in Eq. (3) is the effective PSF of a ZPM.

The values of $h_{x,y,z}$ in the focal plane are displayed for $\lambda = 500$ nm in Figures 3(a), 3(b), and 3(c), respectively. A typical 8%–10% difference in wavelength induced by the Stokes shift has been neglected for simplicity. The FWHM is 100 and 136 nm in the *x* and the *y* direction, respectively. The fact that the FWHM is sharper than in regular confocal microscopy (144 nm in *x* and 128 nm in *y* direction) stems from the fact that marginal rays are employed for illumination, as in annular aperture confocal microscopy. The *yz* section of h_z [Figure 3(d)] demonstrates that the confocalization with a full circular aperture compensates for the axial elongation due to the annular illumination. As a result, the main focal maximum of ZPM is confined to the region around the focus. In Figure 4 we compare the profiles $h_z(x,0,0)$ with $h_x(x,0,0)$ revealing that the contribution from the longitudinal excitation field dominates the signal in the detector.

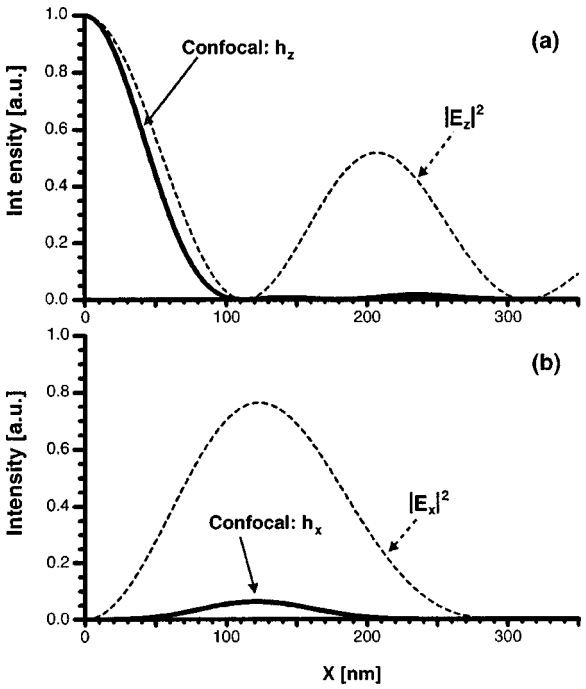

Fig. 4 Profiles for the contribution of the (a) *z*- and (b) *x*-polarized component to the effective PSF of a ZPM (solid lines). The latter vanishes along the optic axis and features an off-axis lobe amounting to 14.0% of that of the main maximum that is entirely dominated by the *z*-polarized field. The dashed lines show the intensity distributions of the field components.

3 Discussion and Conclusion

An advantage of ZPM is the mapping of fluorescence molecules in an object whose transition dipoles are lined up along the optic axis, such as fluorophores in inner or outer membranes of cells. In conjunction with images taken with regular (*x* or *y*) polarized fields, molecular orientation relaxation should be measurable in all directions. If the quantum efficiency of the fluorophore is known, ZPM can be used for quantitative polarization spectrometry and the determination of absolute values of μ_z. As μ_x and μ_y are found by operating the microscope in a conventional manner, one can establish the orientation and the total magnitude of $\boldsymbol{\mu}$ at microscopic scale. The scheme does not require any interferometry so that ZPM should be facile to implement in a regular confocal microscope, where it would emphasize the contribution of *z*-oriented molecules. An important advantage of ZPM over other arrangements with significant longitudinal field components is that its effective PSF is engineered in such a way that the contributions of the undesired transverse components are weakened by the orthogonal orientation of the illumination and detection PSF. This makes ZPM particularly interesting for the imaging of the *z*-polarized features in randomly oriented agglomerations of molecules, as is the case in biomedical microscopy.

The arbitrary change of the field orientation will be equally important to nonlinear interactions of the field with the molecule, as the orientation of the focal field to the first and second order hyperpolarizibility tensors is crucial for the effective generation of nonlinearly induced scattering or fluorescence signals. Therefore, we anticipate that ZPM will also be relevant to multiphoton absorption, higher harmonics, as well as coherent-anti-Stokes Raman scattering imaging spectroscopy at high spatial resolution.

References

1. J. B. Birks, *Organic Molecular Photophysics*, Wiley, New York (1973).
2. E. H. K. Stelzer and S. Lindek, "Fundamental reduction of the observation volume in far-field light microscopy by detection orthogo-

nal to the illumination axis: Confocal theta microscopy,'' *Opt. Commun.* **111**, 536–547 (1994).
3. C. J. R. Sheppard, ''Fundamental reduction of the observation volume in far-field light microscopy by detection orthogonal to the illumination axis: Confocal theta microscopy comment,'' *Opt. Commun.* **119**, 693–694 (1995).
4. J. Sepiol, J. Jasny, J. Keller, and U. P. Wild, ''Single molecule observed by immersion mirror objective. The orientation of terrylene molecules via the direction of its transition dipole moment,'' *Chem. Phys. Lett.* **273**, 444–448 (1997).
5. R. M. Dickson, D. J. Norris, and W. E. Moerner, ''Simultaneous imaging of individual molecules aligned both parallel and perpendicular to the optic axis,'' *Phys. Rev. Lett.* **81**, 5322–5325 (1998).
6. M. A. Bopp, Y. Jia, G. Haran, E. A. Morlino, and R. M. Hochstrasser, ''Single-molelule spectroscopy with 27 fs pulses: Time-resolved experiments and direct imaging of orientational distributions,'' *Appl. Phys. Lett.* **73**(1), 7–9 (1998).
7. E. Betzig and R. J. Chichester, ''Single molecules observed by near-field scanning optical microscopy,'' *Science* **262**, 1422–1425 (1993).
8. S. A. Empedocles, R. Neuhauser, and M. G. Bawendi, ''Three-dimensional orientation measurements of symmetric single chromophores using polarization microscopy,'' *Nature (London)* **399**, 126–130 (1999).
9. B. Richards and E. Wolf, ''Electromagnetic diffraction in opticle systems II. Structure of the image field in an aplanatic system,'' *Proc. R. Soc. London, Ser. A* **253**, 358–379 (1959).
10. H. T. M. van der Voort and G. J. Brakenhoff, ''3D-image formation in high aperture fluorescence confocal microscopy,'' *J. Microsc.* **158**, 43–54 (1990).
11. C. J. R. Sheppard and P. Török, ''An electromagnetic theory of imaging in fluorescence microscopy, and imaging in polarization fluorescence microscopy,'' *Bioimaging* **5**(4), 205–218 (1997).
12. S. W. Hell and E. H. K. Stelzer, ''Fundamental improvement of resolution with a 4Pi-confocal fluorescence microscope using two-photon excitation,'' *Opt. Commun.* **93**, 277–282 (1992).
13. B. Sick, B. Hecht, and L. Novotny, ''Orientational imaging of single molecules by annular illumination,'' *Phys. Rev. Lett.* **85**, 4482–4485 (2000).
14. J. T. Fourkas, ''Rapid determination of the three-dimensional orientation of single molecules,'' *Opt. Lett.* **26**(4), 211–213 (2001).
15. S. Quabis, R. Dorn, M. Eberler, O. Glöckl, and G. Leuchs, ''Focussing light to a tighter spot,'' *Opt. Commun.* **179**, 1–7 (2000).
16. K. S. Youngworth and T. G. Brown, ''Inhomogeneous polarisation in scanning optical microscopy,'' *Proc. SPIE* **3919**, (2000).
17. M. A. Lieb and A. J. Meixner, ''A high numerical aperture parabolic mirror as imaging device for confocal microscopy,'' *Opt. Express* **8**(7), 458–474 (2001).
18. S. W. Hell, ''Increasing the resolution of far-field fluorescence light microscopy by point-spread-function engineering,'' in *Topics in Fluorescence Spectroscopy*, J. R. Lakowicz, Ed., Vol. 5, pp. 361–422, Plenum, New York (1997).
19. S. W. Hell, G. Reiner, C. Cremer, and E. H. K. Stelzer, ''Aberrations in confocal fluorescence microscopy induced by mismatches in refractive index,'' *J. Microsc.* **169**, 391–405 (1993).